

# Applications of photothermal beam deflection calorimetry to organic photochemistry

Syun-Ru Yeh, Daniel E. Falvey \*

*Department of Chemistry and Biochemistry, University of Maryland, College Park, MD 20742, USA*

Received 2 June 1994; accepted 20 September 1994

## Abstract

Photothermal beam deflection calorimetry (PDC) measures the time-dependent heat release that follows optical excitation of a sample. From these measurements, parameters such as reaction enthalpies and rates can be determined. In this work, it is shown that this method can be conveniently applied to the measurement of intersystem crossing quantum yields, triplet energies and photochemical reaction enthalpy changes in a variety of organic molecules. In general, PDC signals are linear with excitation energy and sample concentration. Also, the rates and enthalpies derived from these measurements show good agreement with literature values. In certain cases, a non-linear response of the signal with respect to the excitation energy is observed. This appears to be the result of multiphoton absorption by the sample. Comparison of PDC with complementary photothermal methods, such as photoacoustic calorimetry and thermal lens calorimetry, is discussed.

*Keywords:* Photothermal; Kinetics; Triplet state; Enthalpy; Quantum yields; Laser effects; Solvent effects

## 1. Introduction

The measurement of energy changes in molecular systems is of central importance in understanding chemistry. For stable molecules, enthalpy changes can be determined from the enthalpies of formation ( $\Delta H_f$ ) of the products and reactants. The latter quantities are often available or can be measured easily by microcalorimetry. For short-lived species, such as free radicals, carbenes and electronically excited molecules, the enthalpies are more elusive. For excited states which emit light, the energies can be determined by fluorescence or phosphorescence spectroscopy. For free radicals, the enthalpies are often estimated using bond dissociation energies (BDEs) of model compounds. Unfortunately, many excited state species do not emit light and BDEs are accurate only if the compound of interest is structurally similar to the model system.

Recently, several time-resolved photothermal calorimetric methods have been introduced [1,2]. These include photoacoustic calorimetry (PAC, also known as laser-induced optoacoustic calorimetry (LIOAC)) [3–22], thermal lensing (TL) [23–27] and photothermal grating calorimetry [28]. Such methods have made it

possible to determine the energies of excited states, free radicals [29], carbenes [3,20,21], radical ions [9], *trans*-cycloalkenes [11,30] and other unstable species.

PAC measures  $\Delta H$  by monitoring a pressure wave which is generated as a result of rapid photothermal heating of the sample [14]. Its chief limitation is that the signal is convoluted with instrument response and extracting the kinetic information is difficult and uncertain when a large number of adjustable parameters are employed. TL is another method for obtaining the same data [23–27]. In this case, the refractive index change caused by photothermal heating is used to defocus a probe beam. Limitations of this method include stringent requirements for collinear beam alignment and the need for a gaussian excitation beam profile.

This report describes the application of photothermal beam deflection calorimetry (PDC) to the problem of measuring enthalpies of photophysical and photochemical processes. Like PAC and TL, this experiment measures the photothermal heating of the sample. As with TL, PDC measures the time-dependent changes in the refractive index of the solution caused by pulsed excitation. However, instead of defocusing the probe beam, PDC relies on the thermal lens to direct a probe

\* Corresponding author.

beam into a detector. In an ideal situation, this allows for zero background detection of the signal.

PDC experiments were first described in the early 1980s [31,32]. In the original experiments, the local thermal response of a periodically heated solid surface was detected by the deflection of a probe laser beam passing through the gaseous region adjacent to the heated surface spot. PDC has been applied subsequently to the measurement of the optical properties of opaque solids, liquids and gases [33,34]. Applications to imaging and microscopy have also been explored [35,36]. The signal generation process has been well described from a theoretical perspective [32,37]. Tam et al. [38] have demonstrated the use of PDC for measuring the energy relaxations in  $\text{CS}_2$  and  $\text{NO}_2\text{-N}_2\text{O}_4$  vapors following photoexcitation. Reports by Poston and Harris [39,40], where PDC was successfully applied to the measurement of the O–H BDE in benzophenone ketyl radical, suggested that this method might be generally applicable to photoreactions of organic molecules.

This work demonstrates that transverse excitation PDC can be applied successfully to the study of non-radiative electronic transitions of organic molecules in solution. It is shown that a pulsed excitation source with a non-gaussian beam profile (an excimer laser) can be used for these experiments. Specifically, the apparatus described herein is capable of measuring triplet state lifetimes ( $\tau_T$ ), intersystem crossing quantum yields ( $\phi_{\text{isc}}$ ) and triplet energies ( $E_T$ ). Additionally,  $\Delta H$  for a photochemical reaction, the Norrish type II cleavage of valerophenone, is measured accurately.

## 2. Experimental details

The PDC instrument is shown in Fig. 1. The excitation beam was generated by a pulsed XeCl (308 nm) excimer laser (Questek 2120), attenuated by a beam splitter (1/3) and a liquid filter (2-hydroxybenzophenone- $\text{CH}_3\text{CN}$ ) and then focused onto a quartz cuvette (10 mm  $\times$  10 mm). Before the sample, the excitation beam was sampled (1/10) and monitored with a pyroelectric energy meter (Moletron J50). The excitation power density

was kept below  $5.0 \text{ MW cm}^{-2}$ . The heat release following photoexcitation was probed by a continuous wave (CW) He–Ne laser (Uniphase, 0.5 mW). The probe beam was first expanded by lens 1 to a beam diameter of about 2 cm. It was then refocused by lens 2 onto the sample. Two knife edges were used as spatial filters. A pin hole and a knife edge were placed between the lenses to block the scattered light and half of the beam. Lens 3 was used to focus the beam passing through the sample into a Hamamatsu R928 photomultiplier tube (PMT). A second knife edge was used to block the remaining half beam before lens 3. The net result of this optical configuration was to maximize the sensitivity and minimize the background signal. The output voltage from the PMT was monitored by a LeCroy 9420 digital oscilloscope which was remote controlled by a microcomputer. A total of 100 signals were acquired and averaged for each measurement.

Sample solutions were placed in sealed (10 mm  $\times$  10 mm) cuvettes and purged with  $\text{N}_2$  for 5 min to remove  $\text{O}_2$ . The sample absorbance was kept below 0.1 (through 10 mm) to avoid depth dependence and self-quenching. For comparison, the percentage transmittance of the sample and reference (2-hydroxybenzophenone (2-HBP)) solutions at 308 nm were carefully matched using a Milton Roy MRD 3000 UV–visible diode array spectrophotometer.

## 3. Background

The principle behind PDC is that photolysis of a sample causes local heating in the irradiated zone due to non-radiative decay of the excited states thus created. Local heating results in thermal expansion which, in turn, causes a local decrease in the refractive index ( $n$ ). Thermal lens calorimetry and PDC both rely on this phenomenon to alter the characteristics of a second, probe beam, which is passed through the irradiated zone. For PDC, the variation in the excitation beam profile creates a refractive index gradient which deflects the probe beam away from or towards a detector. This is illustrated in Fig. 2.

Expressions for the deflection angle have been derived by Jackson et al. [41]. These workers were especially interested in a well-behaved gaussian excitation beam profile. This work is concerned with cases where the excitation beam profile does not fit to any easily treated function. In general, the deflection angle  $\Theta(z)$  depends on the temperature distribution ( $\partial T/\partial x$ ), the sensitivity of the refractive index to temperature ( $\partial n/\partial T$ ) and the position in the  $z$  axis at which the probe beam intersects the excitation beam ( $z_0$ )

$$\Theta(z) = \frac{1}{n_0} \frac{\partial n}{\partial T} \frac{\partial T}{\partial x} z_0 \quad (1)$$

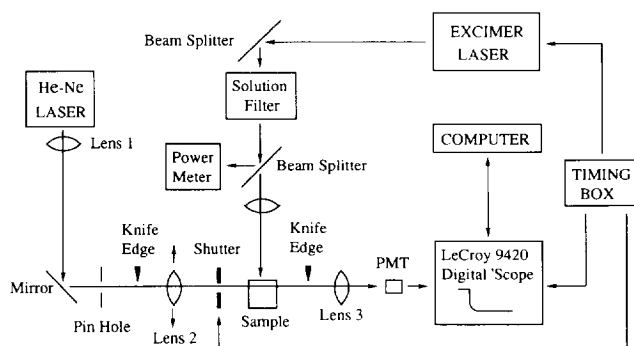


Fig. 1. PDC apparatus used in the experiments.

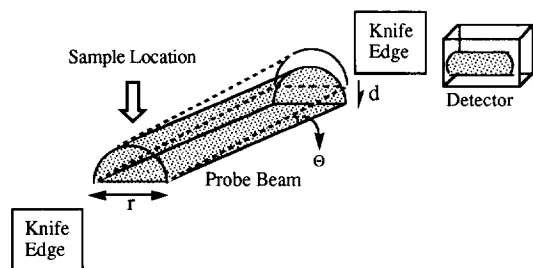


Fig. 2. Detection scheme used in the PDC apparatus. The probe beam is generated from a 0.5 mW He-Ne laser. The first knife edge blocks the bottom edge of the probe beam and the second knife edge blocks the top half. Heat generated from the excitation beam causes the probe beam to bend at angle  $\Theta$  and enter the PMT detector. PDC signals are measured as the relative amount of light entering the detector.

The temperature  $T$  is determined by the absorbed energy of the excitation pulse  $E_{\text{abs}}$ , the specific heat of the solvent  $C_p$ , the solvent density  $\rho$  and the fraction of excitation energy that is converted to heat and the distribution of the excited states created by excitation  $Q(z,t)$

$$\Theta(z) = \frac{E_{\text{abs}}}{n_0 C_p \rho} \frac{\partial n}{\partial z} z_0 \quad (2)$$

The distribution function  $Q(z,t)$  can be separated into a time-dependent part  $r(t)$  and a  $z$ -dependent part  $q(z)$

$$Q(z,t) = r(t)q(z) \quad (3)$$

Strictly speaking,  $r(t)$  depends on two factors. The first is the rate of heat dissipation or heat diffusion from the excitation zone. The latter is easily treated if the beam distribution is gaussian, but only numerically solvable if it is not. For the present purposes, heat dissipation will be neglected. In the experiments described below, the heat dissipation occurs on the order of 10–100 ms, whereas the non-radiative processes of interest occur on microsecond timescales. The second factor in the time dependence is the rate of heat generation. This is determined by the rate constant for each non-radiative process ( $1/\tau_i$ ) and the fraction of excitation energy that is generated in that process  $\alpha_i$

$$r(t) = \sum_{i=0}^k \alpha_i \{1 - \exp(-t/\tau_i)\} \quad (4)$$

The coefficient  $\alpha_i$  is, in turn, determined by the molar enthalpy change for the process  $\Delta H_i$ , its quantum efficiency  $\phi_i$  and the molar energy of the excitation photons  $h\nu_{\text{exc}}$

$$\alpha_i = \frac{\Delta H_i \phi_i}{h\nu_{\text{exc}}} \quad (5)$$

Substituting Eq. (3) into Eq. (2) gives

$$\Theta(z,t) = \frac{E_{\text{abs}}}{n_0 C_p \rho} \frac{\partial n}{\partial T} \left[ \sum_{i=0}^k \alpha_i \{1 - \exp(-t/\tau_i)\} \right] z_0 \quad (6)$$

For organic molecules in solution, often several simplifying approximations can be made [42]. Many of the relaxations occur rapidly relative to the 10 ns duration of the excitation pulse. These can all be treated as time-independent processes with a total amplitude  $\alpha_{\text{fast}}$ . Singlet excited states of organic molecules typically have lifetimes of less than 10 ns, so any process arising from the singlet state will appear as part of  $\alpha_{\text{fast}}$ . Triplet state decays and many other photochemical reactions occur monoexponentially over longer timescales,  $\tau_{\text{slow}}$ . In many situations, Eq. (7) will be adequate to describe the signal behavior

$$\Theta(z,t) = \frac{E_{\text{abs}}}{n_0 C_p \rho} \frac{\partial n}{\partial T} \frac{\partial q}{\partial z} [\alpha_{\text{fast}} + \alpha_{\text{slow}} \{1 - \exp(-t/\tau_{\text{slow}})\}] \quad (7)$$

In principle, a careful measurement of  $\Theta$  would yield the enthalpies of the photochemical and photophysical processes of interest. In practice, the  $\Theta$  values actually used are on the order of milliradians and difficult to measure precisely. Instead, the displacement of the probe beam in the  $z$  direction was monitored by measuring the portion of its light that was deflected past the second knife edge ( $I_{\text{probe}}$ ) (Fig. 2). For small angles,  $\Theta$  can be assumed to be directly proportional to the vertical displacement  $d \sin \Theta$ . Therefore the detected probe beam intensity is given by Eq. (8), where  $B$  is an instrumental parameter that reflects the alignment of the pump and probe beams and converts  $\Theta$  into intensity

$$I_{\text{probe}} = B \frac{E_{\text{abs}}}{n_0 C_p \rho} \frac{\partial n}{\partial T} \frac{\partial q}{\partial z} \times [\alpha_{\text{fast}} + \alpha_{\text{slow}} \{1 - \exp(-t/\tau_{\text{slow}})\}] \quad (8)$$

The heat release from a sample can be determined by comparison of its signal with that of a standard. The most convenient standard is one that converts all of the photon energy into heat within the time window of the excitation pulse ( $\alpha_{\text{fast}} = 1$ ;  $\alpha_{\text{slow}} = 0$ ). Both ferrocene [8] and 2-HBP [29] fulfil these conditions. The enthalpy from the sample can be calculated from the ratio of its signal intensity to that of the standard. Under conditions of identical sample absorbance, excitation energy, temperature, solvent and instrumental alignment, the ratio is given by

$$\frac{I_{\text{sample}}}{I_{\text{std}}} = [\alpha_{\text{fast}} + \alpha_{\text{slow}} \{1 - \exp(-t/\tau_{\text{slow}})\}] \quad (9)$$

The probe beam is circular with a gaussian intensity profile. Consequently, the signal intensity will be a convolution of the probe beam profile and the deflection angle  $\Theta$ . However, the experimental geometry is arranged such that only a small cross-section near the center of the probe beam is used. This is shown in

Fig. 2. At small deflection angles, the intensity should increase linearly with the deflection angle. This assumption is verified by the experiments described below.

## 4. Results and discussion

### 4.1. Signal characteristics

Eqs. (7) and (8) predict a linear dependence of the signal intensity on  $E_{\text{abs}}$ , the absorbed excitation energy. In principle, deviations from this may be caused either by the instrument or by multiphoton absorption by the sample. Instrumental non-linearities would be due to a failure of the assumptions used in the derivation of Eq. (8) (e.g. the  $z$  axis displacement of the probe beam is assumed to be a linear function of  $\Theta$ ) or to the non-uniform shape of the probe beam. Multiphoton absorption by the sample makes the effective  $E_{\text{abs}}$  larger than that predicted by the UV transmittance measurements.

The effects of varying both the sample absorbance and the excitation energy were explored. The dependence on sample absorbance is shown in Fig. 3. With 2-HBP and all other samples examined, good linearity with sample absorbance is observed. This result shows that the deflection angle  $\Theta$  is sufficiently small that non-linearities inherent in the experimental geometry are not significant.

In most cases the signal was found to be linear with excitation energy. However, with certain systems, significant contributions from quadratic terms were observed. The PDC signals from 2-HBP and acetone in  $\text{CH}_3\text{CN}$ , resulting from varying excitation energies, are shown in Fig. 4. With 2-HBP, the signals were linear with pulse energy. By contrast, the signal for acetone showed a non-linear dependence over the same range of pulse energies and at similar signal amplitudes. This behavior is expected for two-photon absorption. If the

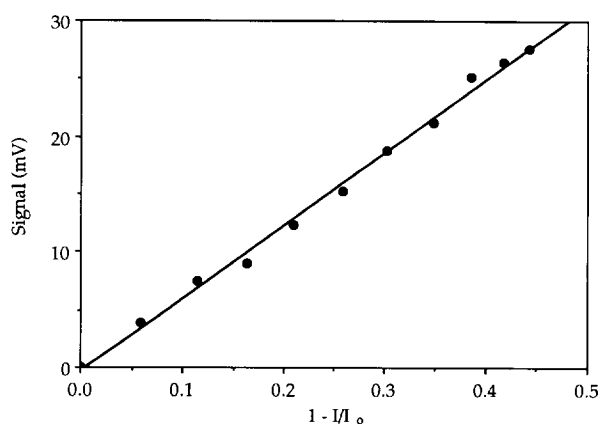


Fig. 3. Dependence of the PDC signal on the concentration of the sample. The ordinate is the fraction of excitation light absorbed by the sample through 10 mm. The sample is 2-HBP in benzene.

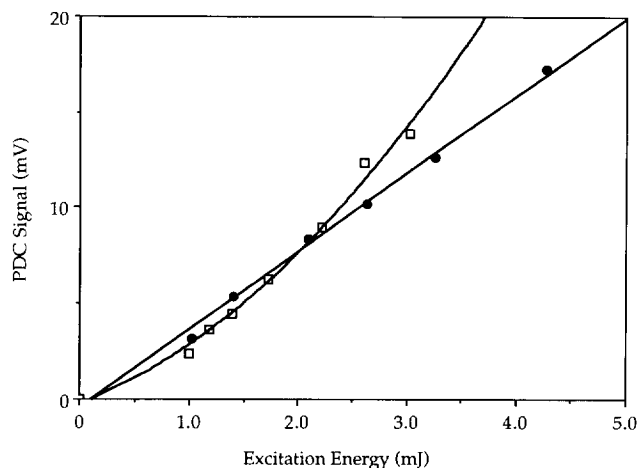


Fig. 4. PDC signals for 2-HBP (filled circles) and acetone (open squares) as a function of excitation energy. In both cases the solvent is benzene and the sample optical density at 308 nm is 0.3.

non-linear behavior was inherent in the instrumental geometry, it would only depend on the deflection angle  $\Theta$ . In that case, all samples would display this effect at the same signal intensity.

Poston and Harris [39] have reported similar effects with PDC experiments on benzophenone in ethanol. In this case, the triplet state of benzophenone is formed rapidly within the duration of the laser pulse and absorbs a second photon at the excitation wavelength (355 nm). The excited triplet state of acetone is formed in 2 ns and has a known absorption band at 300 nm [43]. We propose an analogous effect in the acetone experiment. As a consequence of this finding, all enthalpy determinations were performed by measuring the signal over a range of pulse energies to ensure that contributions from biphotonic or multiphotonic absorption were negligible.

The dependence of the signal on the excitation-probe beam overlap was also explored. According to Eq. (7), the deflection angle  $\Theta$  and, by consequence, the signal amplitude are expected to vary with the heat gradient  $\partial Q/\partial z$ . The latter results from the distribution of photons in the excitation pulse. The measured intensity distribution of the excitation beam along the  $z$  axis is shown in Fig. 5. Along this particular axis the distribution is roughly, but not precisely, gaussian. Based on Eq. (7), a maximum (positive) signal is expected to occur at the positive inflexion point. At the negative inflexion point, the probe beam will be directed away from the detector, towards the knife edge, resulting in a large negative signal. At the center of the excitation beam,  $\partial q/\partial z = 0$  and no deflection should be observed. As shown in Fig. 5, there is good agreement between the predicted and observed behavior. For all of the measurements, the alignment was empirically adjusted to give a maximum positive signal for the reference compound.

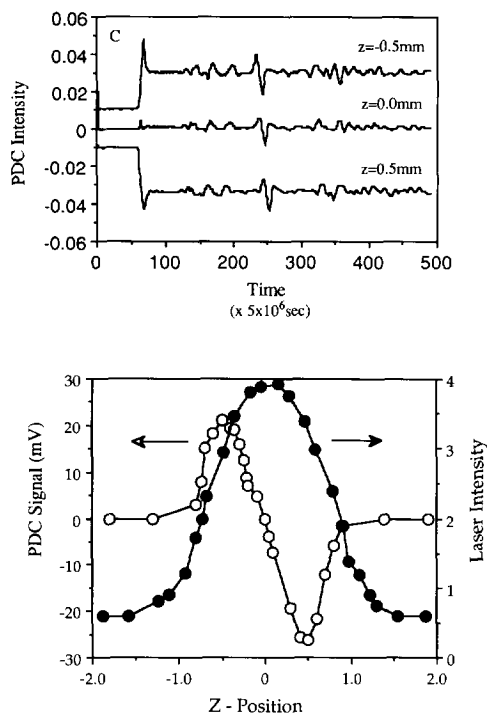


Fig. 5. Effect of beam alignment on the PDC signal. The top panel shows the PDC signals for 2-HBP in benzene as a function of the  $z$  axis position (perpendicular to the optical bench). The spikes after the laser pulse and at  $50 \mu\text{s}$  are due to the accompanying acoustic wave and its reflection. The bottom panel shows a plot of the PDC signal intensity and excitation beam intensity along the  $z$  axis.

In interpreting the time-dependent behavior, it is assumed that the rate of heat dissipation is slow relative to the rate of the slowest signal formation ( $1/\tau_{\text{slow}}$ ). For a gaussian distribution of heat, the decay of the signal should follow [37]

$$I = \frac{1}{n_0} \frac{\partial n}{\partial T} \frac{8\alpha E_0}{\pi} \frac{z}{\sqrt{2\pi\rho C_p}} \times (a^2 + 8Dt)^{3/2} \exp\left\{\frac{-2z}{(a^2 + 8Dt)}\right\} \quad (10)$$

This assumes that the heat is generated rapidly relative to diffusion. Given a beam radius of  $0.5 \text{ mm}$  ( $a/2$ ) along the  $z$  axis (where it is the narrowest) and a thermal diffusivity  $D = 1.70 \times 10^{-7} \text{ m}^2 \text{ s}^{-1}$  in the solvent  $\text{CH}_3\text{CN}$ , and monitoring the decay at the inflexion point ( $z = a/2$ ), the diffusion is predicted to occur with a half-time of  $300 \text{ ms}$ . Fig. 6 shows that, in practice, the decay occurs somewhat faster than this, with a half-time of about  $30 \text{ ms}$ . This could be due to convection. In any case, the measurement of any process that occurs on a submillisecond timescale may be considered without reference to heat diffusion. Most triplet decays and many photochemical processes of interest occur in the nanosecond to microsecond time regime.

Finally, the effect of solvent on the signals was examined. Eq. (7) predicts that the signal will be

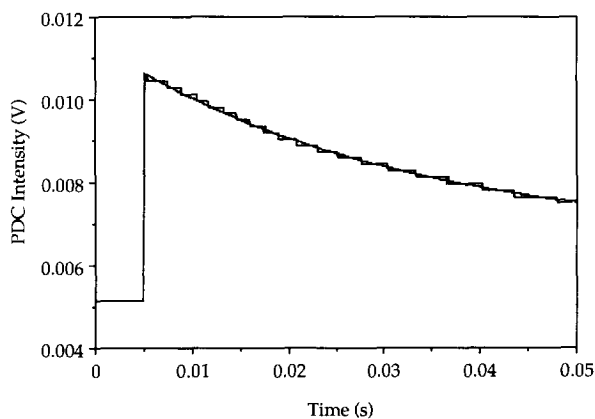


Fig. 6. Decay of the PDC signal for 2-HBP in  $\text{CH}_3\text{CN}$ .

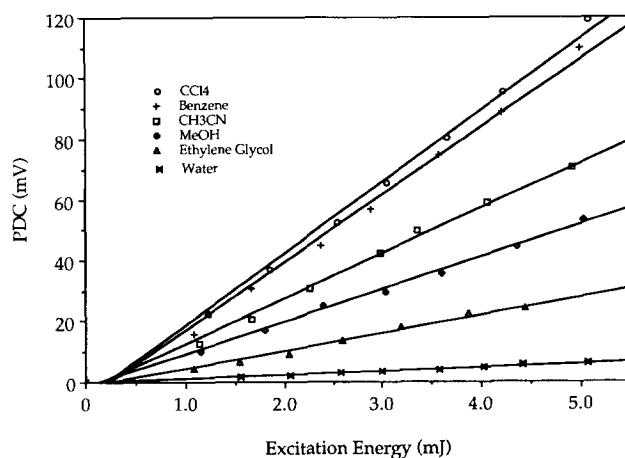


Fig. 7. PDC sensitivities of various solvents. The sample is 2-HBP and the absorbance at  $308 \text{ nm}$  for each sample was carefully matched. The data are compiled in Table 1.

Table 1  
Properties of various solvents and relative PDC sensitivities based on Eq. (7) and measured 2-HBP signals

Solvent	$(\partial n/\partial T)/C_p\rho n_0^a$ (literature)	$(\partial n/\partial T)/C_p\rho n_0^a$ (this work)
Water	(1.0)	(1.0)
Ethylene glycol	4.9	4.7
Methanol	9.2	8.4
Acetonitrile	12.8	11.8
Benzene	17.6	17.7
Carbon tetrachloride	18.4	18.7

<sup>a</sup> Sensitivity relative to water calculated from the individual factors in Ref. [44].

inversely proportional to the density  $\rho$ , the specific heat  $C_p$  and the index of refraction  $n_0$ . The signal amplitude should be directly proportional to  $\partial n/\partial T$ . For many liquids, these parameters are available [44]. In Fig. 7, the PDC signal response for 2-HBP in various solvents is shown. The values in Table 1 were determined by measuring the slopes of the signal vs. pulse energy plots for each solvent. The relative responses vary in

the predicted fashion with solvent. Non-polar, organic solvents, having lower specific heats and densities, generally give the largest signals. For example,  $\text{CCl}_4$  and benzene are almost 20 times more sensitive for these measurements than water.

#### 4.2. Singlet state decay

For organic molecules in solution which do not undergo photochemical reactions, the behavior can be described by Eqs. (11)–(17) [42]. Absorption of the excitation photons promotes the molecule  $M$  into an unrelaxed singlet state  $M^{**}$ ; this rapidly relaxes to the lowest vibrational level of the first excited singlet state  $M^*$ . The  $M^*$  state can return to the ground state either by fluorescence, internal conversion or the triplet state  $M^{3*}$



The triplet state can decay either by phosphorescence or by intersystem crossing. In solution at room temperature, phosphorescence quantum yields are typically very low. Therefore, in most cases, Eq. (17) can be neglected. In this case, the only process which will cause  $\alpha$  to differ from unity will be fluorescence. For such situations, the heat efficiency can be estimated using

$$\alpha_{\text{total}} = \frac{(E_{\text{exc}} - E_s \Phi_f)}{E_{\text{exc}}} \quad (18)$$

Eq. (18)

where  $E_{\text{exc}}$  is the excitation energy ( $87 \text{ kcal mol}^{-1}$ ) and  $E_s$  and  $\Phi_f$  are the singlet energy and the fluorescence quantum yield of the sample respectively. It should be noted that the amount of energy loss due to fluorescence is not exactly equal to the singlet state energy  $E_s$ . Fluorescence can occur to excited vibrational states of the ground electronic state. Consequently, Eq. (18) should tend to underestimate  $\alpha_{\text{total}}$  slightly. For molecules with large Stokes shifts, this could be significant.

The non-radiative efficiency  $\alpha$  is obtained by comparing the PDC signal with that of 2-HBP. The PDC signal amplitudes of anthracene, tryptophan and pyrene in benzene solution are shown in Fig. 8. The  $\alpha$  values measured with the present apparatus, together with those estimated using Eq. (18), are shown in Table 2. It should be noted that  $\alpha + \Phi_f = 1$  only when the energy

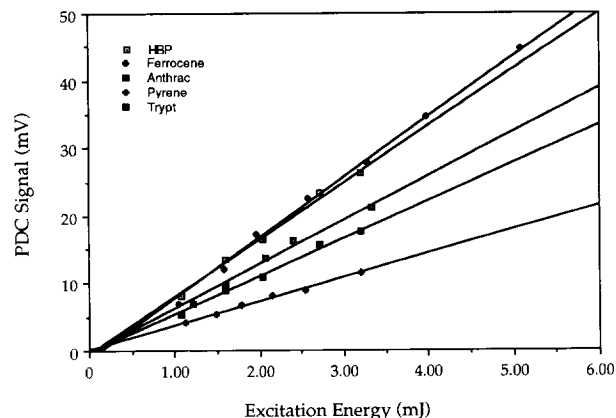


Fig. 8. PDC signals for 2-HBP, ferrocene, anthracene, pyrene and tryptophan. The data are compiled in Table 2.

Table 2

Singlet energy ( $E_s$ ), fluorescence quantum yield ( $\Phi_f$ ) and heat release efficiency ( $\alpha$ ) for the standard compounds

Sample	$E_s^a$ (eV)	$\Phi_f^a$	$\alpha$ (literature)	$\alpha$ (this work)
2-HBP	—	0	(1.00)	(1.00)
Ferrocene	—	0	1.00	$0.99 \pm 0.02$
Anthracene	3.31	0.27	0.78	$0.78 \pm 0.02$
Tryptophan	4.08	0.20 <sup>b</sup>	0.80 <sup>b</sup>	$0.67 \pm 0.02^c$
Pyrene	3.33	0.70	0.42	$0.42 \pm 0.02$

<sup>a</sup> From Ref. [44].

<sup>b</sup> This value was measured in aqueous solution.

<sup>c</sup> The solvent is  $\text{CH}_3\text{OH}$ .  $\alpha$  was calculated by comparison with 2-HBP in the same solvent.

of the lowest excited singlet state is equal to the excitation photon energy. In most cases, relaxation within the excited singlet manifold (Eq. (12)) will add to the total signal. Good agreement between the literature values for  $E_s \Phi_f$  and those obtained from the PDC experiment shows that the technique is useful for characterizing these non-radiative processes.

#### 4.3. Triplet state decay

For certain organic compounds, the rate of intersystem crossing  $k_{isc}$  is fast relative to other singlet decay channels. In these cases, a significant fraction of the excited molecules reach the triplet state  $M^{3*}$  and the heat is evolved from the system on a much longer timescale than that of singlet processes. In normal cases, the singlet processes occur in several nanoseconds or less, and the triplet decays occur over timescales of several microseconds to several seconds. Under such circumstances, PDC can resolve temporally the singlet decays (Eqs. (12)–(15)) from the triplet decay (Eq. (16)).

Fig. 9 shows the PDC signal obtained from the pulsed excitation of anthracene in  $\text{CH}_3\text{CN}$ . There is an initial jump in the signal that corresponds to the sum of the

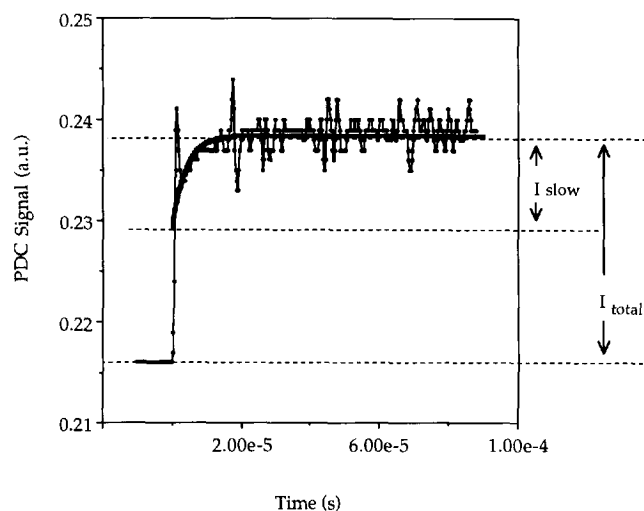


Fig. 9. PDC waveform from anthracene showing an initial jump due to singlet decay processes and a slow rise due to non-radiative decay of the triplet state. The spikes at  $t=0$  and  $20 \mu\text{s}$  are due to the acoustic pressure wave and its reflection.

heat generated in the singlet processes. The slower rise, which has a time constant of  $9 \mu\text{s}$ , is due to decay of the triplet. The latter is in reasonable agreement with the literature lifetime of  $11 \mu\text{s}$ . The time resolution in these experiments is limited by the transit of the acoustic wave which occurs as a consequence of sample excitation. This is seen as a sharp spike immediately after excitation. The data points associated with this artifact were ignored when fitting the risetimes. In practice, the acoustic wave limits the time resolution of the present apparatus to  $500 \text{ ns}$ .

For triplet decay, the ratio of the slow heat release ( $\alpha_{\text{slow}}$ ) to the total heat release ( $\alpha_{\text{total}}$ ) can be described by

$$\frac{I_{\text{slow}}}{I_{\text{total}}} = \frac{\alpha_{\text{slow}}}{\alpha_{\text{total}}} = \frac{E_t \Phi_t}{(E_{\text{exc}} - E_s \Phi_r)} \quad (19)$$

The advantage of the PDC technique is that  $\phi_{\text{isc}}$  can be obtained by direct observation. For these determinations, reference to an external standard is not necessary: the total heat release can be used as an internal standard. PDC signals were obtained from anthracene, benzil, phthalazine and tetramethylbenzidine. The  $\Phi_t$  values calculated using Eq. (19), as well as the literature values, are shown in Table 3.

#### 4.4. Norrish type II cleavage of valerophenone

Finally, the PDC technique was applied to a system which undergoes an irreversible photochemical reaction. Ketones are one of the most well-studied functional groups in organic chemistry. These species undergo a variety of photoreactions. The Norrish type II cleavage reaction is a unimolecular process which occurs when the triplet excited carbonyl group abstracts an H atom

from the alkyl chain. The resulting triplet diradical fragments rapidly to give an alkene and a ketone (Scheme 1). Valerophenone (1-phenylpentanone) has been shown to fragment with a quantum yield of unity in polar solvents [45].

$$\alpha_{\text{total}} = \frac{(E_{\text{exc}} - \Delta H_r \Phi_r)}{E_{\text{exc}}} \quad (20)$$

In Fig. 10, the pulse energy dependence of the deflection amplitude for valerophenone in  $\text{CH}_3\text{CN}$  is shown together with the 2-HBP standard. The product of the molar enthalpy and quantum yield of the process,  $\Delta H_r \Phi_r$ , can be calculated from Eq. (20).  $E_{\text{exc}}$  is the molar energy of the excitation photons. The measured parameter  $\alpha_{\text{total}}$  is obtained from the ratio of the valerophenone signal to that for 2-HBP under identical conditions of beam alignment, temperature, sample absorbance, etc.  $\Delta H_r$  thus calculated is  $16 \pm 6 \text{ kcal mol}^{-1}$ . This is in reasonable agreement with the value of  $18 \text{ kcal mol}^{-1}$  measured by Rudzki et al. [5] using PAC. Because of the timescale limitations associated with the acoustic wave, we were unable to resolve the diradical and measure its rate of fragmentation.

The formation of stable, neutral products is predicted to have a negligible contribution to the deflection signal. For example, in  $\text{CH}_3\text{CN}$ , under typical conditions (3 mJ excitation energy, optical density of 0.5 through 1 cm at 308 nm and an experimental volume of  $2.5 \mu\text{l}$ ), the change in the index of refraction due to heating would be

$$\Delta n_{\text{heat}} = \frac{E_{\text{abs}}}{n_0 C_p \rho V_{\text{exp}}} \frac{\partial n}{\partial T} = 7.19 \times 10^{-5}$$

The change in the index of refraction due to the change in stable solute will be several orders of magnitude smaller. The number of stable product molecules is limited by the number of photons absorbed in the irradiated volume. This corresponds to  $4.15 \times 10^{-10} \text{ mol}$  given the typical conditions stated above. The number of solvent molecules in the same volume is  $1.17 \times 10^{-4} \text{ mol}$  ( $\text{CH}_3\text{CN}$ ). Assuming weak interactions between the solute and the solvent, the total index of refraction for the sample is expected to be determined from the sum of the indices of refraction  $n$  weighted by their mole fractions in the mixture  $\chi$ . Assuming a quantum yield of unity for the chemical reaction (i.e.  $\chi_{\text{photon}} = \chi_{\text{react}} - \chi_{\text{prod}}$ ) and a difference in refractive index between the products and the reactants of 0.1 (typical organic liquids have refractive indices that range from about 1.38 to 1.48) [46], we obtain

$$\Delta n_{\text{chem}} \approx \chi_{\text{photon}} (n_{\text{prod}} - n_{\text{react}}) = 3.5 \times 10^{-7}$$

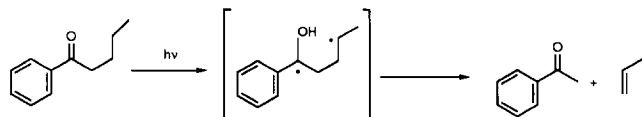
The change in chemical composition should therefore contribute less than 1% to the signal. It is, however, important to realize that the above estimates assume

Table 3

Singlet energy ( $E_s$ ), fluorescence quantum yield ( $\Phi_f$ ), triplet lifetime ( $\tau$ ) of anthracene, benzil, *N,N,N,N*-tetramethylbenzidine (TMB) and phthalazine. The last two columns are the calculated triplet yields ( $\Phi_t$ ) and their literature values

Sample	$E_s^a$ (eV)	$\Phi_f^a$	$E_t^a$ (eV)	$\tau$ ( $\mu$ s) (this work)	$E_t\Phi_t$ (eV) (this work)	$\Phi_t$ (this work)	$\Phi_t^a$ (literature)
Anthracene	3.31	0.27	1.82	4	1.27	$0.70 \pm 0.01$	0.75
Benzil	2.56	0.001	2.32	8	2.04	$0.88 \pm 0.01$	0.92
TMB	3.60	0.56 <sup>a</sup>	2.68	9	1.47	$0.55 \pm 0.01$	0.52
Phthalazine	–	0	2.81	2	1.35	$0.48 \pm 0.01$	0.49

<sup>a</sup> From Ref. [44].



Scheme 1.

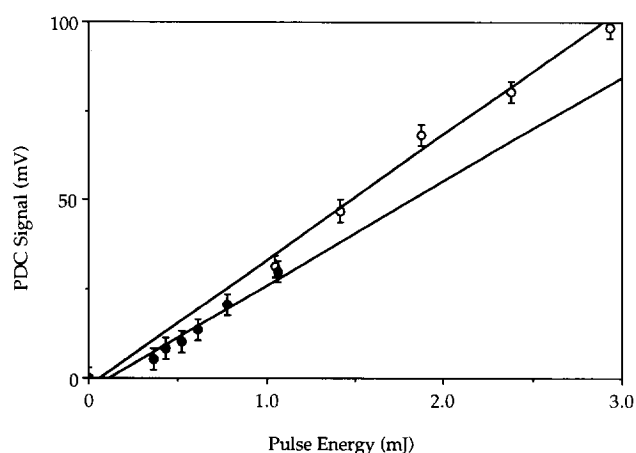


Fig. 10. The PDC signal for 2-HBP (open circles) and valerophenone (filled circles) in  $\text{CH}_3\text{CN}$ .

that the solutes do not interact strongly with the solvent. This condition can break down in cases where the products and reactants interact differently with the solvent. For example, if ions are created from neutrals in a polar solvent, electrostriction will alter the solvent density and subtract from the signal, possibly in a significant way.

## 5. Conclusions

PDC is shown to be a convenient alternative to PAC for measuring enthalpy changes associated with photochemical and photophysical reactions. One advantage is that the rate of the process can be determined directly from the temporal profile of the signal. The time resolution of the present apparatus is limited to about 500 ns by the width of the photoacoustic wave. This is sufficient for the analysis of most triplet lifetimes and should allow for measurement of the rates of

moderately rapid photochemical reactions. Another advantage of PDC is that, unlike thermal lens methods, a gaussian excitation beam is not required. Therefore excimer lasers can be used as the excitation source.

## Acknowledgments

This work was supported by the National Institutes of Health (GM-45856). We thank Mr. David Laman for assistance in preparing the manuscript.

## References

- [1] A.C. Tam, *Rev. Mod. Phys.*, **58** (1986) 381–431.
- [2] S.E. Braslavsky and G.E. Heibel, *Chem. Rev.*, **92** (1992) 1381–1410.
- [3] J.D. Simon and K.S. Peters, *J. Am. Chem. Soc.*, **105** (1983) 5156–5158.
- [4] L.J. Rothberg, J.D. Simon, M. Bernstein and K.S. Peters, *J. Am. Chem. Soc.*, **105** (1983) 3464–3468.
- [5] J.E. Rudzki, J.L. Goodman and K.S. Peters, *J. Am. Chem. Soc.*, **107** (1985) 7849–7854.
- [6] I.V. Katalnikov, M. van der Auweraer and F.C. de Schryver, *J. Photochem. Photobiol. A: Chem.*, **77** (1994) 103–107.
- [7] J.L. Goodman, K.S. Peters and V. Vaida, *Organometallics*, **5** (1986) 815–816.
- [8] J.L. Goodman, K.S. Peters, H. Misawa and R.A. Caldwell, *J. Am. Chem. Soc.*, **108** (1986) 6803–6805.
- [9] J.L. Goodman and K.S. Peters, *J. Am. Chem. Soc.*, **108** (1986) 1700–1701.
- [10] J.L. Goodman and M.S. Herman, *Chem. Phys. Lett.*, **163** (1989) 417–420.
- [11] C. Brennan and R.A. Caldwell, *Photochem. Photobiol.*, **53** (1991) 165–168.
- [12] C.M. Brennan, R.A. Caldwell, J.E. Elbert and D.J. Unett, *J. Am. Chem. Soc.*, **116** (1994) 3460–3464.
- [13] M. Bernstein, J.D. Simon and K.S. Peters, *Chem. Phys. Lett.*, **100** (1983) 241–244.
- [14] K.S. Peters, *Pure Appl. Chem.*, **58** (1986) 1263–1266.
- [15] K.S. Peters and G.J. Snyder, *Science (Washington, DC)*, **241** (1988) 1053–1057.
- [16] J. Westrick, K.S. Peters, J.D. Ropp and S.S. Sligar, *Biochemistry*, **29** (1990) 6741–6746.
- [17] J.A. Westrick and K.S. Peters, *Biophys. Chem.*, **37** (1990) 73–79.
- [18] G.K. Yang, *Chem. Phys. Lett.*, **125** (1986) 566–568.
- [19] K. Marr and K.S. Peters, *Biochemistry*, **30** (1991) 1254–1258.
- [20] J.A. LaVilla and J.L. Goodman, *J. Am. Chem. Soc.*, **111** (1989) 712–714.

- [21] J.A. LaVilla and J.L. Goodman, *Tetrahedron Lett.*, 29 (1988) 2623–2629.
- [22] J.A. Lavilla and J.L. Goodman, *Chem. Phys. Lett.*, 141 (1987) 149–153.
- [23] M. Terazima and T. Azumi, *Chem. Phys. Lett.*, 141 (1987) 237–240.
- [24] M. Terazima and T. Azumi, *Chem. Phys. Lett.*, 145 (1988) 286–289.
- [25] M. Terazima and T. Azumi, *J. Am. Chem. Soc.*, 111 (1989) 3824–3826.
- [26] G. Rossbroich, N.A. Garcia and S.E. Braslavsky, *J. Photochem. Photobiol.*, 31 (1985) 37–48.
- [27] R.W. Redmond, K. Heihoff, S.E. Braslavsky and T.G. Truscott, *Photochem. Photobiol.*, 45 (1987) 209–213.
- [28] M. Terazima, K. Okamoto and N. Hirota, *Laser Chem.*, 13 (1994) 169–185.
- [29] T.J. Burkey, M. Majewski and D. Griller, *J. Am. Chem. Soc.*, 108 (1986) 2218–2221.
- [30] R.A. Caldwell, W. Tang, D.I. Schuster and G. Heibel, *Photochem. Photobiol.*, 53 (1991) 159–164.
- [31] A.C. Boccara, D. Fournier and J. Badoz, *Appl. Phys. Lett.*, 36 (1980) 130–139.
- [32] J.C. Murphy and L.C. Aamodt, *J. Appl. Phys.*, 51 (1980) 4580–4587.
- [33] J.C. Loulergue and A.C. Tam, *Appl. Phys. Lett.*, 46 (1985) 457–459.
- [34] J.D. Spear and R.E. Russo, *J. Appl. Phys.*, 70 (1991) 580–586.
- [35] M. Woelker, B.K. Bein, J. Pezl and H.G. Walther, *J. Appl. Phys.*, 70 (1991) 603–610.
- [36] L.C. Aamodt and J.C. Murphy, *J. Appl. Phys.*, 54 (1983) 581–591.
- [37] R. Gupta, in J.A. Sell (ed.), *Photothermal Investigations of Solids and Fluids*, Academic Press, San Diego, CA, 1989, pp. 82–126.
- [38] A.C. Tam, H. Sontag and P. Hess, *Chem. Phys. Lett.*, 120 (1985) 280–284.
- [39] P.E. Poston and J.M. Harris, *J. Am. Chem. Soc.*, 112 (1990) 644–650.
- [40] P.E. Poston and J.M. Harris, *J. Photochem. Photobiol. A: Chem.*, 60 (1991) 51–61.
- [41] W.B. Jackson, N.M. Amer, A.C. Boccara and D. Fournier, *Appl. Opt.*, 20 (1981) 1333–1344.
- [42] A. Gilbert and J. Baggott, *Essentials of Molecular Photochemistry*, CRC Press, Boca Raton, FL, 1991.
- [43] G. Porter, R.W. Yip, J.M. Dunston, A.J. Cessna and S.E. Sugamori, *Faraday Trans.*, 67 (1971) 3149–3154.
- [44] S.E. Braslavsky and K. Heinoff, in J.C. Scaiano (ed.), *Handbook of Organic Photochemistry*, Vol. 1, CRC Press, Boca Raton, FL, 1989, pp. 327–355.
- [45] P.J. Wagner, *Acc. Chem. Res.*, 4 (1971) 168–177.
- [46] S.L. Murov, I. Carmichael and G.L. Hug, *Handbook of Photochemistry*, Marcel Dekker, New York, 1993.